



On controlling, vibration performance and energy transfer of an offshore wind turbine tower system via PPF controller

Ateq Alsaadi^{1,*}, Y. S. Hamed¹

¹*Department of Mathematics and Statistics, College of Science, Taif University, P. O. Box 11099, Taif 21944, Saudi Arabia*

Abstract. In this paper, we focus on the control, energy transfer, and vibration performance under multi mixed excitations for the offshore wind turbine tower (OWTT) system. For reducing the controlled system oscillations, the positive position feedback (PPF) controller is applied. The energy transfers occur in the system of wind turbine by adding the PPF controller to the system equations. With the help of the phase plane approach, frequency response equations, and Poincare maps, the bifurcation and stability at worst resonance cases are sought and investigated. The vibration behaviors are studied numerically at different parameters values for the wind turbine system. Additionally, the response and numerical outcomes are examined, also, the approach of multiple scales is used to establish the approximate solutions of the wind turbine-controlled system. Besides that, MAPLE and MATLAB algorithms are used to implement the numerical results and compare analytical solutions with numerical behavior. The results also be compared to previous research that has been published.

2020 Mathematics Subject Classifications: 34A34, 34C15, 34C23, 34C25, 34D20, 34E13, 37N15, 70B05, 70K05, 70K40, 70K42, 70K50

Key Words and Phrases: Offshore wind turbine system, Energy transfer, Vibration control, Stability, positive position feedback control

1. Introduction

Renewable energy has grown in importance as a topic of these investigations over the past few decades. On a worldwide scale, the demand for energy has been steadily rising. This increase motivates us to start looking at alternative energy production strategies. One of the most difficult issues our society is currently experiencing is the creation of a sustainable and renewable energy economy. The cost of wind energy has been the main motivator for the shift. Wind energy is projected to contribute significantly in terms of renewable energy in the coming decades to reach such an energy source. By about a third

*Corresponding author.

DOI: <https://doi.org/10.29020/nybg.ejpam.v16i4.4929>

Email addresses: ateq@tu.edu.sa (A. Alsaadi), yasersalah@tu.edu.sa (Y. S. Hamed)

since 2009, wind turbine prices have fallen. Production of wind energy is one of the most effective conservation projects [1, 2]. The Rayleigh's energy approach and ANSYS FSI analysis are used to determine the dynamic effects of the blades on the tower as well as the effects of the earthquake forces, wave, and wind on wind turbine dynamic behavior [3]. Several parameters' effects on the behavior of the (OWTT) system and the responses of the soil monopile tower system are the subject of this investigation [4]. The standard model of large rotating wind turbines active observer with effective control approach is studied [5]. A tuned mass damper and passive control approach are used to study the vibrations of the nacelle of offshore wind turbines and spar oscillations [6]. The effects of an active control method are investigated for a hybrid mass damper and a barge floating wind turbine type [7]. Mathematical analysis study for the wind turbines dynamics with time scale simulations and control was performed [8]. The wind turbines structural vibrations and its high oscillations was suppressed through active controller and has been proposed in [9]. With two different approaches, the environmental forces and seismic loads effect on the offshore wind tower behavior is performed [10]. The transfer the energy and reducing the high oscillations amplitudes of the wind turbine system using both PD and NPD controller are well studied. Furthermore, the Poincaré maps and averaging method were used to study the bifurcation analysis and stability at the worst resonance cases. Additionally, the wind turbine system's frequency and force response curves were drawn before and after the addition of the control unit. In addition, the Numerical simulations were carried out and control parameters performances on the vibration magnitudes was performed applying with Maple and MATLAB algorithms. Obtained results demonstrate the efficiency of the NPD controller in reducing the nonlinear wind oscillations [11-12]. To eliminate the oscillator's van der pol duffing with mixed excitations, the nonlinear integral positive position feedback (NIPPF), and integral resonant (IRC) controllers are applied. The multiple time scales approach and frequency response equations are used to perform the approximate solutions and stability analysis at the worst resonance cases [13]. The detailed of analysis is founded for some dynamical systems with different forces in the books [14-17]. The model of atomic force microscopy (AFM) was controlled utilizing the PD controller with time delayed and the PD control efficiency for putting down the nonlinear oscillations are performed to the obtained results [18]. The controlling of a rotating blade's oscillation via nonlinear saturation control, the energy transfer and stability using technique of Lyapunov's linearization are investigated [19]. The PPF and PD signals control are merged to minimize the levels of AMBs system vibration involving constant stiffness and 16 poles. Also, Approximate solutions are extracted, and response curves are plotted before and after using PPF [20]. 2D and 3D Visualizations of the mass-damper-spring model was controlled with a servo controlled linear actuator (SCLA) with using signal generating (PPF) controller. In addition, they derived the system equations, phases and amplitudes using Krylov-Bogoliubov averaging perturbation method [21]. The approximate solutions, stability, and control for the car model with the harmonic balance and averaging methods with nonlinear saturation controller (NSC) controller a cubic-position negative-velocity and a cubic-position negative-velocity feedback (CPNV) controllers [22-23]. The mathematical methods are presented and explained for obtaining approximate

analytical solutions to differential and difference equations that cannot be solved exactly. The mathematical methods discussed in this book are known collectively as asymptotic and perturbative analysis [24]. The stability analysis of even multidimensional strongly nonlinear systems described by PDEs are studied [25]. Tuned mass and liquid column dampers are used to reduce the excessive vibration responses of offshore wind turbines [26]. A tuned mass damper with passive control in a floating platform can reduce and improve the dynamic responses of the offshore wind turbine [27]. The high frequency tuned mass damper installed in the nacelle is examined using numerical methods to see whether it effectively reduces tower response while having little effect on platform response [28]. A new technique for minimizing the motion of a two-degree-of-freedom tuned mass damper is applied for offshore wind turbines on floating spar supports [29]. Using an electromagnetic shunt tuned mass damper, floating offshore wind turbine vibration can be reduced [30]. According to the articles described above, none of them discuss controlling the primary and internal resonance response via the positive position feedback (PPF) controller, which was the main motive of such a response. The current work suggests using this control approach. In the present work, we focused on the control, energy transfer, and vibration performance under multi mixed excitations for the system of offshore wind turbine tower. For reducing the controlled system oscillations and energy transfers, the PPF controller be applied. With the help of the phase plane approach, frequency response equations, and Poincare maps, the bifurcation and stability at worst resonance cases are sought and investigated. The vibration behaviors are studied numerically at different parameters values for the wind turbine system.

2. System modelling

The parts of the OWTT system are the hub, blade, tower, and concentrated mass. This system is investigated in terms of some excitation forces as in Fig. 1(a). As in Figure 1(b), the structural model with multiple external forces, including the effects of wave F_H , earthquake F_{eqk} , and wind F_{aero} forces.

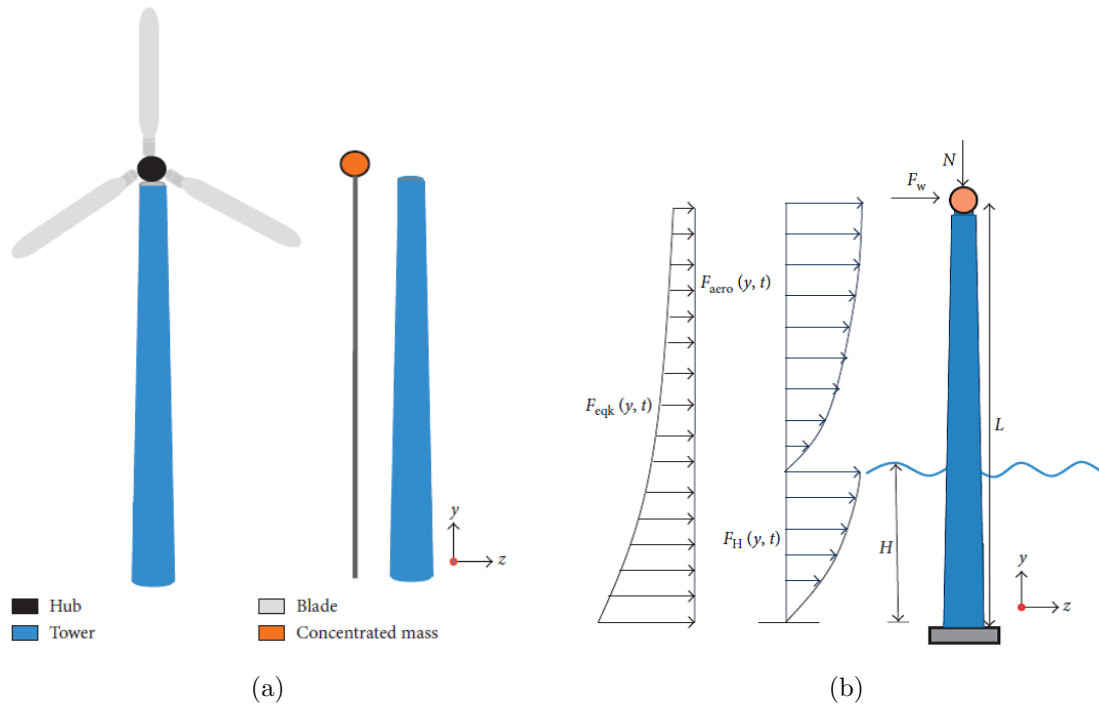


Figure 1: (a) The wind turbine tower model, (b) The wind tower's forces.

The wind forces F_{aero} acting on the Rotor Nacelle Assembly (RNA) and associate instrumentation can be considered as concentrated forces (hydrodynamic forces) which depend on the wind velocity. The wave force F_H were utilized to compute the hydrodynamic wave forces acting on the wind tower, where the wave height H , wavelength L , and wave period T are the major wave parameters. The strong force acting on the turbine tower structure is the earthquake force due to the seismic excitation. The below equation governing the SDOF system's equation of motion, which was obtained from [10]:

$$m\ddot{z}(t) + \epsilon c\dot{z}(t) + kz(t) + \epsilon F(t) = \epsilon G(t) \tag{1a}$$

Where $\ddot{z}(t)$ is the acceleration, $\dot{z}(t)$ is the velocity, $z(t)$ is the coordinate vector, $F(t)$ is the total force, $G(t)$ is controller signal, m is the mass, c and k are the damping and stiffness coefficients, respectively. As proceeding in Ref [10], then the system's equation of motion is derived and modified by the next ordinary differential equation:

$$\ddot{z}\epsilon\mu_1\dot{z} + \omega_1^2 z + \epsilon f_{eqk} + \epsilon f_a \sin \Omega_1(t) = \epsilon f_h \cos \Omega_1(t) |\cos \Omega_1(t)|. \tag{1b}$$

Where $\mu_1 = \frac{c}{m}$, $\omega_1^2 = \frac{k}{m}$, $F(t) = \frac{1}{m}(F_{eqk} + F_{aero} \sin \omega_1(t))$, $G(t) = \frac{1}{m}(F_H \cos \omega_1(t) |\cos \omega_1(t)|)$. Applying the positive position feedback (PPF) controller donate by equation (2b) to the wind turbine tower system in equation (1b). In order to control the oscillation of the tower system, the control unit must acquire the feedback signal from the tower system,

the updated equation (1b) would be as follows:

$$\ddot{z} + \epsilon\mu_1 z + \omega_1^2 z + \epsilon f_a \sin(\omega_1(t)) = \epsilon f_h \cos(\omega_1(t)) |\cos(\omega_1(t))| + \epsilon\beta_1 y. \tag{2a}$$

$$\ddot{y} + \epsilon\mu_2 y + \omega_2^2 y = \epsilon\beta_2 z. \tag{2b}$$

Where μ_1, μ_2 are linear damping factors of the system and control unit, ϵ is small perturbation, f_a, f_h are excitation wind and wave forces, $f_{eqk} = \alpha \cos(\pi t)$ is earthquake force, ω_1, ω_2 are natural frequencies tower system and control unit, ω_1 is the excitation frequency and β_1, β_2 are control units.

3. Approximate analytical solution

The goal of perturbation methods is to propose approximately analytical solutions to problems that do not have exact solutions depending on a small parameter ϵ where $0 \ll \epsilon \ll 1$. During the solution process, (unwanted) secular terms are eliminated using the new independent variables. The latter applies solvability conditions, which are constraints on the approximate solution. Approximate solutions of problem (2) are produced using the Multiple Scale Perturbation (MSP) approach [14-17], and the solutions have the following form:

$$z(t, \epsilon) = z_0(T_0, T_1) + \epsilon z_1(T_0, T_1) + O(\epsilon^2) \tag{3a}$$

$$y(t, \epsilon) = y_0(T_0, T_1) + \epsilon y_1(T_0, T_1) + O(\epsilon^2) \tag{3b}$$

We provide the derivatives in the following format:

$$\frac{d}{dt} = \begin{cases} D_0 + \epsilon D_1, \\ \frac{d^2}{dt^2} = D_0^2 + 2\epsilon D_0 D_1. \end{cases} \tag{3c}$$

where $T_0 = t, T_1 = \epsilon t$ and $D_0 = \frac{\partial}{\partial T_0}, D_1 = \frac{\partial}{\partial T_1}$ are the time scales and derivatives respectively and substituting equations (3a) (3b) through (3c) into equation (2), we get

$$\begin{aligned} & (D_0^2 z_0 + \omega_1^2 z_0) + \epsilon(D_0^2 z_1 + \omega_1^2 z_1 + 2D_0 D_1 z_0 + \mu_1 D_0 z_0 + \alpha \cos(\pi T_0) + f_a \sin(\Omega_1 T_0) \\ & - f_h \cos(\Omega_1 T_0) |\cos(\Omega_1 T_0)| - \beta_1 y_0) + \epsilon^2(D_0^2 z_2 + \omega_1^2 z_2 + 2D_0 D_1 z_1 + D_1^2 z_0 - f_h \cos(\Omega_1 T_0) \\ & |\cos(\Omega_1 T_0)| - \beta_1 y_0) + \epsilon^2(D_0^2 z_2 + \omega_1^2 z_2 + 2D_0 D_1 z_1 + D_1^2 z_0 + \mu_1(D_1 z_0 + D_0 z_1) - \beta_1 y_1) = 0. \end{aligned} \tag{4a}$$

$$(D_0^2 y_0 + \omega_2^2 y_0) + \epsilon(D_0^2 y_1 + \omega_2^2 y_1 + 2D_0 D_1 y_0 + \mu_2 D_0 y_0 - \beta_2 z_0) + \epsilon^2(D_0^2 y_2 + \omega_2^2 y_2 + 2D_0 D_1 y_1 + D_1^2 y_0 + \mu_2(D_1 y_0 + D_0 y_1) - \beta_2 z_1) = 0. \tag{4b}$$

Equating the coefficients of ϵ in equation (4) leads: $O(\epsilon^0)$:

$$(D_0^2 + \omega_1^2)z_0 = 0. \tag{5a}$$

$$(D_0^2 + \omega_2^2)y_0 = 0. \tag{5b}$$

$O(\epsilon^1)$:

$$(D_0^2 + \omega_1^2)z_1 = -2D_0D_1z_0 - \mu_1D_0z_0 - \alpha \cos(\pi T_0) - f_a \sin(\omega_1 T_0) + f_h \cos^2(\omega_1 T_0) + \beta_1 y_0, \quad \cos(\omega_1 T_0) \geq 0. \tag{6a}$$

or

$$(D_0^2 + \omega_1^2)z_1 = -2D_0D_1z_0 - \mu_1D_0z_0 - \alpha \cos(\pi T_0) - f_a \sin(\omega_1 T_0) - f_h \cos^2(\omega_1 T_0) + \beta_1 y_0, \quad \cos(\omega_1 T_0) < 0. \tag{6b}$$

$$(D_0^2 + \omega_2^2)y_1 = -2D_0D_1y_0 - \mu_2D_0y_0 + \beta_2 z_0. \tag{6c}$$

Equation (5) has a general solution expressed as:

$$z_0 = A_1(T_1)e^{i\omega_1 T_0} \bar{A}_1(T_1)e^{-i\omega_1 T_0}. \tag{7a}$$

$$y_0 = A_2(T_1)e^{i\omega_2 T_0} + \bar{A}_2(T_1)e^{-i\omega_2 T_0} \tag{7b}$$

Substituting equation (7) into equation (6), the following are obtained:

$$(D_0^2 + \omega_1^2)z_1 = [-i\omega_1(2D_1A_1 + \mu_1A_1)]e^{i\omega_1 T_0} + [i\omega_1(2D_1\bar{A}_1 + \mu_1\bar{A}_1)]e^{-i\omega_1 T_0} + \beta_1 A_2 e^{i\omega_2 T_0} + \beta_1 \bar{A}_2 e^{-i\omega_2 T_0} + (if_a)/2(e^{i\Omega_1 T_0} - e^{-i\Omega_1 T_0}) + \frac{f_h}{4}(e^{2i\Omega_1 T_0} + e^{-2i\Omega_1 T_0} + 2) - \frac{\alpha}{2}e^{i\pi T_0} - \frac{\alpha}{2}e^{-i\pi T_0}, \quad \cos(\Omega_1 T_0) \geq 0. \tag{8a}$$

or

$$(D_0^2 + \omega_1^2)z_1 = [-i\omega_1(2D_1A_1 + \mu_1A_1)]e^{i\omega_1 T_0} + [i\omega_1(2D_1\bar{A}_1 + \mu_1\bar{A}_1)]e^{-i\omega_1 T_0} + \beta_1 A_2 e^{i\omega_2 T_0} + \beta_1 \bar{A}_2 e^{-i\omega_2 T_0} + (if_a)/2(e^{i\Omega_1 T_0} - e^{-i\Omega_1 T_0}) + \frac{f_h}{4}(e^{2i\Omega_1 T_0} + e^{-2i\Omega_1 T_0} + 2) - \frac{\alpha}{2}e^{i\pi T_0} - \frac{\alpha}{2}e^{-i\pi T_0}, \quad \cos(\Omega_1 T_0) < 0. \tag{8b}$$

$$(D_0^2 + \omega_2^2)y_1 = [-i\omega_2(2D_1A_2 + \mu_1A_2)]e^{i\omega_2 T_0} + [i\omega_2(2D_1\bar{A}_2 + \mu_1\bar{A}_2)]e^{-i\omega_2 T_0} + \beta_1 A_1 e^{i\omega_2 T_0} + \beta_1 \bar{A}_1 e^{-i\omega_2 T_0}. \tag{8c}$$

After the secular terms $e^{(\pm i\omega_1 T_0)}$ and $e^{(\pm i\omega_2 T_0)}$ were eliminated from equations (8a) -(8c), the general solutions given as

$$z_1 = (A_3 e^{i\omega_1 T_0} + \bar{A}_3 e^{i\omega_1 T_0}) + \frac{\beta_1}{(\omega_1^2 - \omega_2^2)} (A_2 e^{i\omega_2 T_0} + \bar{A}_2 e^{-i\omega_2 T_0}) + \frac{(if_a)}{2} (\omega_1^2 - \Omega_1^2) (e^{i\Omega_1 T_0} - e^{-i\Omega_1 T_0}) + \frac{fh}{4} (\omega_1^2 - 4\Omega_1^2) (e^{2i\Omega_1 T_0} + e^{-2i\Omega_1 T_0}) + \frac{fh}{(2\omega_1^2)} - \frac{\alpha}{2} (\omega A_1^2 - \pi^2) (e^{i\pi T_0} + e^{-i\pi T_0}). \tag{9a}$$

or

$$z_1 = (A_3 e^{i\omega_1 T_0} + \bar{A}_3 e^{i\omega_1 T_0}) + \frac{\beta_1}{(\omega_1^2 - \omega_2^2)} (A_2 e^{i\omega_2 T_0} + \bar{A}_2 e^{-i\omega_2 T_0}) + \frac{(if_a)}{2} (\omega_1^2 - \Omega_1^2) (e^{i\Omega_1 T_0} - e^{-i\Omega_1 T_0}) - \frac{fh}{4} (\omega_1^2 - 4\Omega_1^2) (e^{2i\Omega_1 T_0} + e^{-2i\Omega_1 T_0}) - \frac{fh}{(2\omega_1^2)} - \frac{\alpha}{2} (\omega_1^2 - \pi^2) (e^{i\pi T_0} + e^{-i\pi T_0}). \tag{9b}$$

$$y_1 = (A_4 e^{i\omega_2 T_0} + \bar{A}_4 e^{-i\omega_2 T_0}) + \frac{\beta_2}{(\omega_2^2 - \omega_1^2)} (A_1 e^{i\omega_1 T_0} + \bar{A}_1 e^{-i\omega_1 T_0}). \tag{9c}$$

The resonances were obtained from the approximations and are given as follows:

- a . Primary, super-harmonic and Internal resonance are: $\Omega_1 \cong \pm\omega_1, \Omega_1 \cong \pm\omega_1 2$ and $\omega_1 \cong \pm\omega_2$.
- b With any combination of the above resonance cases, simultaneous resonance is obtained.

Analysis and studies are done on the solution’s stability in the primary with internal resonance case $\Omega_1 \cong \omega_1, \omega_1 \cong \omega_2$, Where the detuning σ_1 and σ_2 are given as:

$$\Omega_1 = \omega_1 + \epsilon\sigma_1, \omega_2 = \omega_1 + \epsilon\sigma_2. \tag{10}$$

The first order approximation’s solvability conditions are given by inserting equation (10) into equation (8a) -(8b) and removing the secular then we get:

$$-i\omega_1 (2D_1 A_1 + \mu_1 A_1) + \beta_1 A_2 e^{i\sigma_2 T_1} + \frac{(if_a)}{2} e^{i\sigma_1 T_1} = 0. \tag{11a}$$

$$-i\omega_2(2D_1A_2 + \mu_2A_2) + \beta_1A_1e^{(-i\sigma_2T_0)} = 0. \tag{11b}$$

Let's introduce the polar form as:

$$A_1 = \frac{1}{2}a_1(T_1)e^{i\phi_1(T_1)}, A_2 = \frac{1}{2}a_2(T_1)e^{i\phi_2(T_1)} \tag{12}$$

where ϕ_1, ϕ_2 are the motion's phases and a_1, a_2 are the amplitudes steady state. By inserting equation (12) into equations (11a)–(11b) and equating the real and imaginary parts, the modulation of the phases and amplitudes is achieved, and the result is as follows.

$$\dot{a}_1 = \frac{-\mu_1a_1}{2} + \frac{(\beta_1a_2)}{2\omega_1 \sin \theta_2} + \frac{f_a}{2\omega_1} \cos \theta_1 \tag{13a}$$

$$a_1\dot{\phi}_1 = \frac{-\beta_1a_2}{2\omega_1 \cos \theta_2} + \frac{f_a}{2\omega_1} \sin \theta_1 \tag{13b}$$

$$\dot{a}_2 = \frac{-\mu_2a_2}{2} - \frac{\beta_2a_1}{2\omega_2} \sin \theta_2 \tag{14a}$$

$$a_2\dot{\phi}_2 = \frac{-\beta_2a_1}{2\omega_2} \cos \theta_2 \tag{14b}$$

Where

$$\theta_1 = \sigma_1T_1 - \phi_1, \theta_2 = \sigma_2T_1 - \phi_1 + \phi_2 \tag{15}$$

From equation (15) we have

$$\dot{\phi}_1 = \sigma_1 - \dot{\theta}_1, \dot{\phi}_2 = \sigma_2 - \sigma_1 - \dot{\theta}_2 + \theta_1 \tag{16}$$

Substituting equation (16) into equations (13a) -(14b), we obtained

$$\dot{a}_1 = \frac{-\mu_1a_1}{2} + \frac{\beta_1a_2}{2\omega_1} \sin \theta_2 + \frac{f_a}{(2\omega_1)} \cos \theta_1. \tag{17a}$$

$$a_1\dot{\theta}_1 = a_1\sigma_1 + \frac{\beta_1a_2}{2\omega_1} \cos \theta_2 - \frac{f_a}{2\omega_1} \sin \theta_1 \tag{17b}$$

$$\dot{a}_2 = \frac{-\mu_2a_2}{2} - \frac{\beta_2a_1}{2\omega_2} \sin \theta_2 \tag{18a}$$

$$a_2\dot{\theta}_2 = a_2\sigma_2 - \frac{\beta_2a_1}{2\omega_2} \cos \theta_2 + \frac{\beta_1a_2^2}{2\omega_1a_1} \cos \theta_2 - \frac{f_aa_2}{2\omega_1a_1} \sin \theta_1 \tag{18b}$$

It is too difficult to find the solutions of equations (17) and (18) analytically, but we can obtain the solutions numerically. To obtain the approximate periodic solutions, substituting equations (7a), (7b) and (12) into equations (3a), (3b) and neglecting terms of $o(\epsilon)$, we have

$$z = \frac{1}{2}a_1e^{i(\omega_1T_0+\phi_1)} + \frac{1}{2}a_1e^{-i(\omega_1T_0+\phi_1)} \tag{19a}$$

$$y = \frac{1}{2}a_2e^{i(\omega_2T_0+\phi_2)} + \frac{1}{2}a_2e^{-i(\omega_2T_0+\phi_2)} \tag{19b}$$

We can write the first approximation periodic solution in the form:

$$z = a_1 \cos(\Omega_1 T_0 - \theta_1) \tag{20a}$$

$$y = a_2 \cos(\Omega_1 T_0 + \theta_2 - \theta_1) \tag{20b}$$

where a_1, a_2, θ_1 and θ_2 are the solutions of the equations (17) and (18) at the steady state.

4. Stability investigations

To get vibration amplitudes of the steady state, we set $\dot{a}_1 = \dot{a}_2 = \dot{\theta}_1 = \dot{\theta}_2 = 0$, into equations (17a) -(18b), we get:

$$\frac{\mu_1 a_1}{2} = \frac{\beta_1 a_2}{2\omega_1} \sin \theta_2 + \frac{f_a}{2\omega_1} \cos \theta_1 \tag{21a}$$

$$a_1 \sigma_1 = \frac{-\beta_1 a_2}{2\omega_1} \cos \theta_2 + \frac{f_a}{2\omega_1} \sin \theta_1 \tag{21b}$$

$$\frac{\mu_2 a_2}{2} = -\frac{\beta_2 a_1}{2\omega_2} \sin \theta_2 \tag{22a}$$

$$a_2(\sigma_2 - \sigma_1) = \frac{\beta_2 a_1}{2\omega_2 \cos \theta_2}. \tag{22b}$$

Eliminating θ_1 and θ_2 from equations (21) and (22) leads to:

$$a_1^2 = \frac{\omega_2^2}{\beta_2^2} (\mu_2^2 + 4(\sigma_2 - \sigma_1)^2) a_2^2. \tag{23}$$

$$\frac{f_a^2}{4\omega_1^2} = \left(\frac{\mu_1 a_1}{2} + \frac{\beta_1 a_2^2 \mu_2 \omega_2}{2\beta_2 a_1 \omega_1} \right)^2 + \left(\sigma_1 a_1 + \frac{\beta_1 a_2^2 \omega_2}{\beta_2 a_1 \omega_1} (\sigma_2 - \sigma_1) \right)^2. \tag{24}$$

Equations (23) and (24) are the frequency-response equations for the system steady-state behavior at the practical case ($a_1, a_2 \neq 0$). By computationally resolving the above algebraic problem using the Newton-Raphson technique, we can get the steady state solution of equations (2a) and (2b). Using Lyapunov’s direct method [15], the solution stability is evaluated. Assume the following equation:

$$a_n = a_{n0} + a_{n1} \text{ and } \theta_n = \theta_{n0} + \theta_{n1} (n = 1, 2). \tag{25}$$

Where a_{n0} and a_{n1} are perturbative and steady-state amplitudes. Similarly, θ_{n0} and θ_{n1} are perturbative phases and steady-state phases. Inserting equation (25) into equations (17-18) and linearizing give us

$$\begin{pmatrix} \dot{a}_{11} \\ \dot{\theta}_{11} \\ \dot{a}_{21} \\ \dot{\theta}_{21} \end{pmatrix} = \mathbf{J} \begin{pmatrix} a_{11} \\ \theta_{11} \\ a_{21} \\ \theta_{21} \end{pmatrix} = \begin{pmatrix} r_{11} & r_{12} & r_{13} & r_{14} \\ r_{21} & r_{22} & r_{23} & r_{24} \\ r_{31} & r_{32} & r_{33} & r_{34} \\ r_{41} & r_{42} & r_{43} & r_{44} \end{pmatrix} \begin{pmatrix} a_{11} \\ \theta_{11} \\ a_{21} \\ \theta_{21} \end{pmatrix}$$

where \mathbf{J} is the Jacobian matrix, and its constituent parts are listed in the appendix. \mathbf{J} is defining equation of a fourth-degree equation in the following form.

$$\lambda^4 + R_1\lambda^3 + R_2\lambda^2 + R_3\lambda + R_4 = 0 \quad (26)$$

where R_i ($i=1, \dots, 4$) are listed in the appendix. The roots of equation (26) are the eigenvalues of \mathbf{J} and they determine whether the system solutions are stable or not. The system's periodic solution is unstable if the real part of the eigenvalue is positive; if not, the system becomes stable. The Routh-Hurwitz criterion demonstrates that the roots of equation (26) had negative real parts, If and only if the following equation holds true:

$$R_1 > 0, R_1R_2 - R_3 > 0, R_3(R_1R_2 - R_3) - R_1^2R_4 > 0, R_4 > 0 \quad (27)$$

5. Discussion on the primary and internal resonance curves

As it has been concluded in equations (23) and (24) that there two cases:

- 1 . $(a_1, a_2 \neq 0)$ where the controller is active.
- 2 . $(a_1, a_2 = 0)$ where the controller is inactive.

The system parameters are given by $\mu_1 = 0.04, \mu_2 = 0.02, \beta_1 = 5, \beta_2 = 0.5, \alpha = 9.73, \Omega_1 = 1.26, \omega_1 = 1.26, \omega_2 = 1.26, f_a = 67.17, f_h = 5.129$.

5.1. Effect of some important different parameters on the wind tower system before control

In this part, we looked at how various parameters affected the behavior of the wind tower system before control. The system behavior is shown in Figures 2(a, b) as a monotonically decreasing function of the damping coefficient μ_1 and a monotonically increasing function in the excitation wind force f_a .

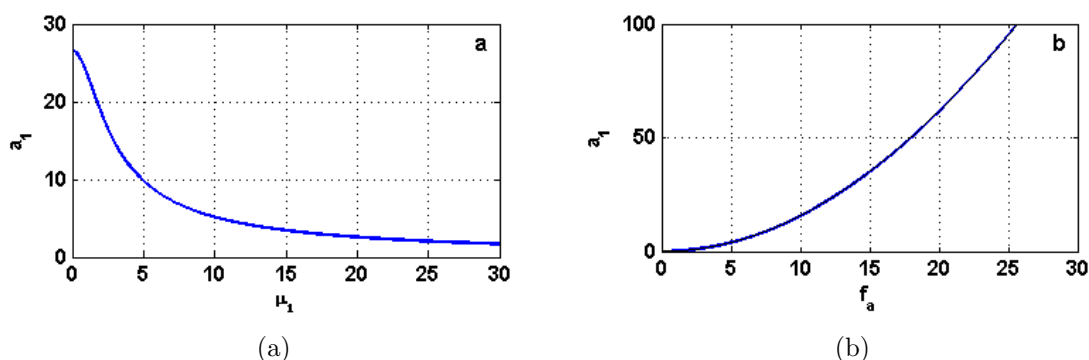


Figure 2: (a) Effect of linear damping μ_1 , (b) Effect of excitation wind force f_a on wind tower system response.

5.2. Curves of force and frequency response for the system without control

The equilibrium behavior of the wind turbine tower amplitude a_1 in terms of the forcing amplitude f_a before control ($\beta_1 = 0, \beta_2 = 0$) is shown in Fig. 3. As the parameters μ_1 and ω_1 are increased, the stable nontrivial amplitudes decreased. In Fig. 4 (a, b, c), the equilibrium behavior of the amplitude a_1 in terms of the frequency detuning σ_1 is plotted before control ($\beta_1 = 0, \beta_2 = 0$). In this figure, increasing the parameters μ_1 and ω_1 can reduce the oscillations of the system, but the oscillations is increased with the increase the parameters f_a .

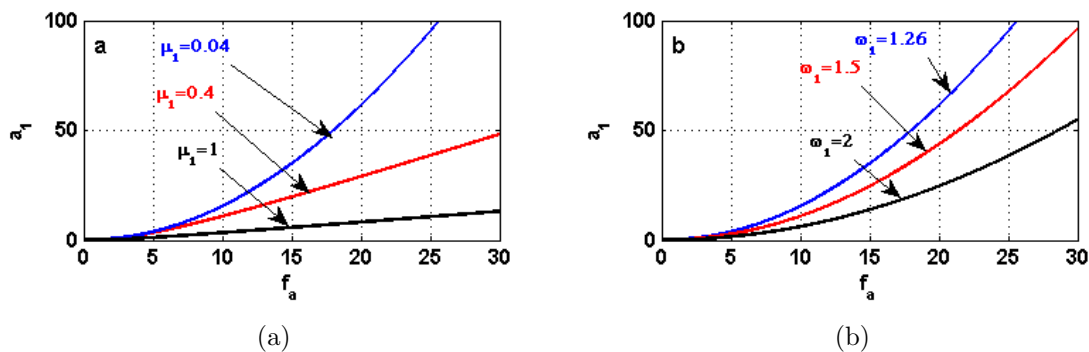


Figure 3: (a) Curves of force response for OWTT system before control ($\beta_1 = 0, \beta_2 = 0$) at different values of linear damping μ_1 , (b) Curves of force response for OWTT system before control ($\beta_1 = 0, \beta_2 = 0$) at different values of natural frequency ω_1 .

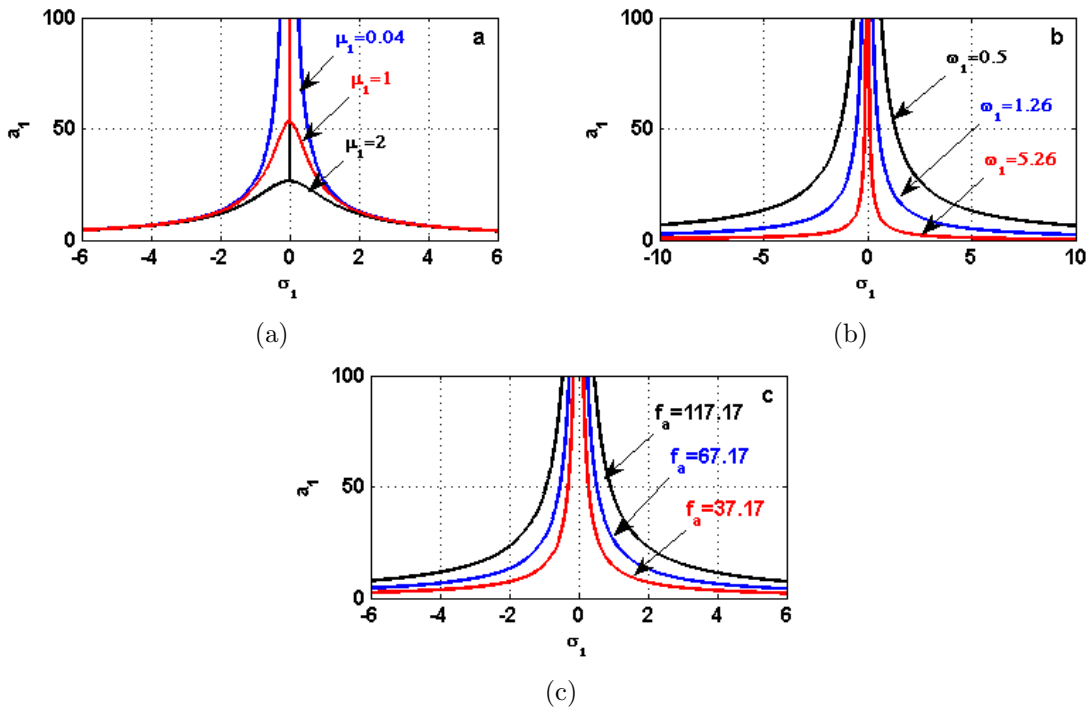


Figure 4: (a) Curves of force response for OWTT system before control ($\beta_1 = 0, \beta_2 = 0$) at different values of linear damping μ_1 , (b) Curves of force response for OWTT system before control ($\beta_1 = 0, \beta_2 = 0$) at different values of natural frequency ω_1 , (c) Curves of force response for OWTT system before control ($\beta_1 = 0, \beta_2 = 0$) at different values of wind amplitude force f_a .

5.3. Curves of frequency response for the controlled system

Using frequency response curves, we investigated the effects of the various factors on the controlled system’s stability zone. In Figs. (5-10), the equilibrium behavior of the (WTT)amplitudes a_1, a_2 in terms of the frequency detuning σ_1 is plotted before control ($\beta_1 = 5, \beta_2 = 0.5$). According to Fig. 5, the controlled system behavior is a monotonically increasing function in the parameter f_a . Figures (6–8) demonstrate the controlled system’s behavior as a monotonic decreasing function of the parameters μ_1, μ_2, ω_1 and ω_2 . We utilize these parameters to reduce the oscillations of the OWTT system based on these figures. Additionally, the saturation occurs, and the curves are shifted to the right for the system behavior with the change in values β_1, β_2 , but the control behavior is decreased with increasing β_1 and increased with increasing β_2 as shown in Figs. (9, 10).

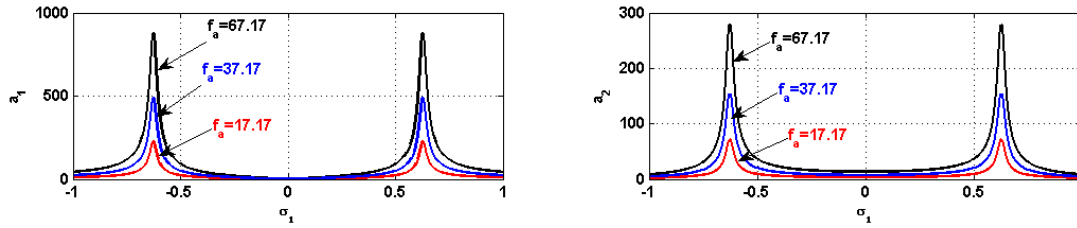


Figure 5: Curves demonstrating the controlled system’s frequency response after control ($\beta_1 = 5, \beta_2 = 0.5$) at different values of wind amplitude force f_a .

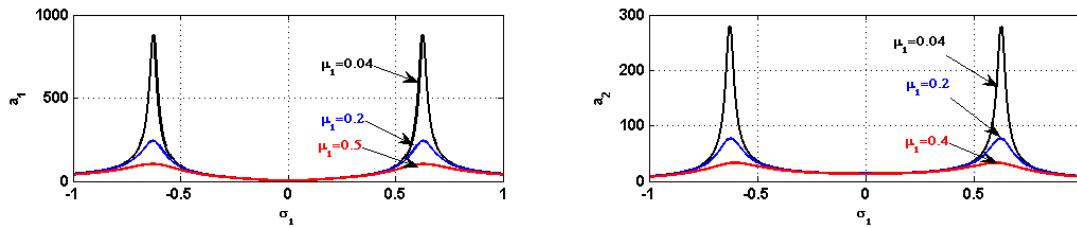


Figure 6: Curves demonstrating the controlled system’s frequency response after control ($\beta_1 = 5, \beta_2 = 0.5$) at different values of linear damping μ_1 .

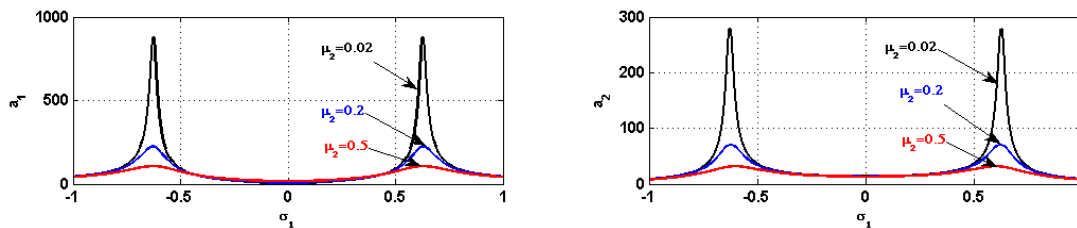


Figure 7: Curves demonstrating the controlled system’s frequency response after control ($\beta_1 = 5, \beta_2 = 0.5$) at different values of linear damping μ_2 .

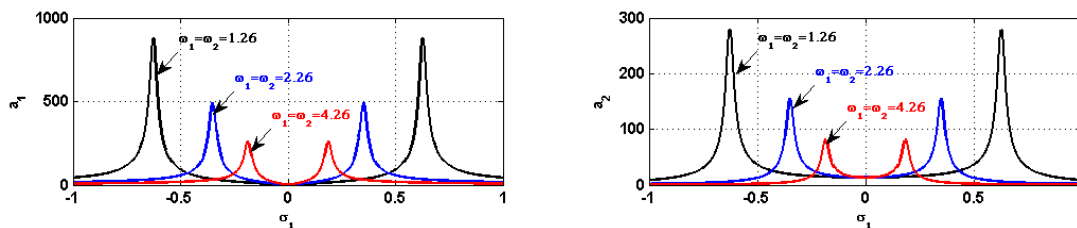


Figure 8: Curves demonstrating the controlled system’s frequency response after control ($\beta_1 = 5, \beta_2 = 0.5$) at different values of natural frequencies ω_1, ω_2 .

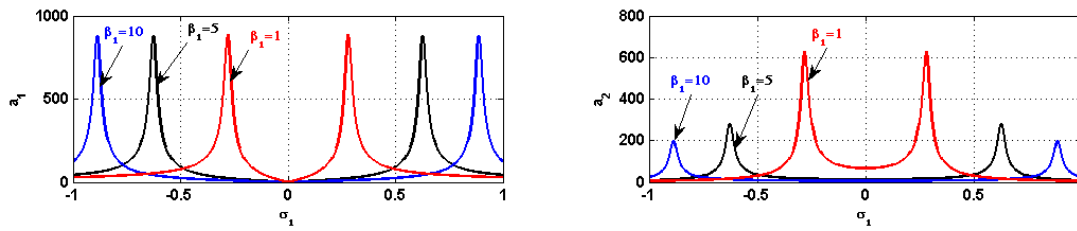


Figure 9: Curves demonstrating the controlled system’s frequency response after control ($\beta_1 = 5, \beta_2 = 0.5$) at different values of control unit β_1 .

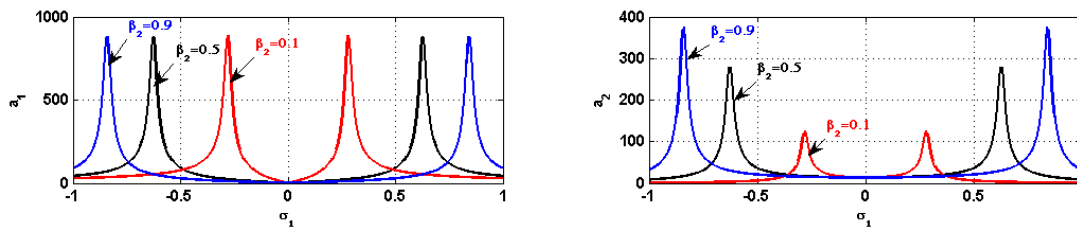


Figure 10: Curves demonstrating the controlled system’s frequency response after control ($\beta_1 = 5, \beta_2 = 0.5$) at different values of control unit β_2 .

6. Discussion of analytical and numerical results

Using the fourth order Rung-Kutta numerical approach, Figures 11 to 14 simulate the wind turbine tower vibrations both before and after control. In terms of time before control, Figure 11 shows the wind turbine tower’s nontrivial vibrations. Figure 11(a) depicts the system oscillations, which have an amplitude of about 43 centimeters, while Figure 11(b) depicts a steady-state system oscillation of last 20 seconds to demonstrate the reader the specifics of the solution waveform. Additionally, the controlled system’s oscillation amplitude can reach 0.6 centimeters, and the unit control’s effectiveness ($E_a =$ the amplitude before control/amplitude after control) equal $E_a=72$ when ($\beta_1 = 5, \beta_2 = 0.5, \omega_1 = 1.26$) as shown in Fig. 12, this mean that the steady oscillations of the wind turbine had been reduced from their former state by about 98.5. Also, the oscillation amplitude of the controlled system can reach approximately 7 centimeters and $E_a=6.2$ when ($\beta_1 = 5, \beta_2 = 0.05, \omega_1 = 1.26$) as shown in Fig 13, and reach approximately 1 centimeters and $E_a=43$ when ($\beta_1 = 5, \beta_2 = 0.5, \omega_1 = 2.01$) as shown in Fig. 14. In According to Fig. 15, with the addition of a PPF controller, energy is moved from the system before control to the system after control and the performance of PPF control is more effective at the primary and internal resonance case $\Omega_1 \approx \omega_1 \approx \omega_2$ with small values of values ω_1 and ω_2 .

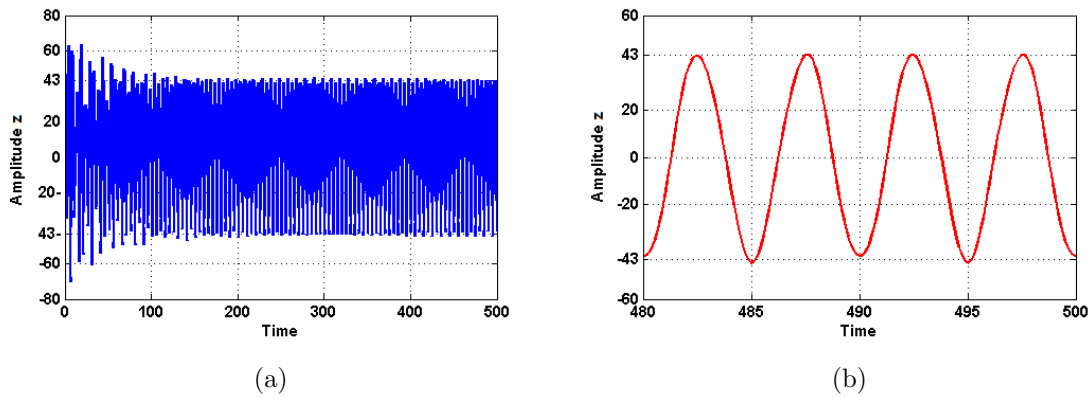


Figure 11: The OWTT vibrations before control at $\beta_1 = 0, \beta_2 = 0, \omega_1 = 1.26$ (a) all-round response, (b) last 20 seconds of the all-round response

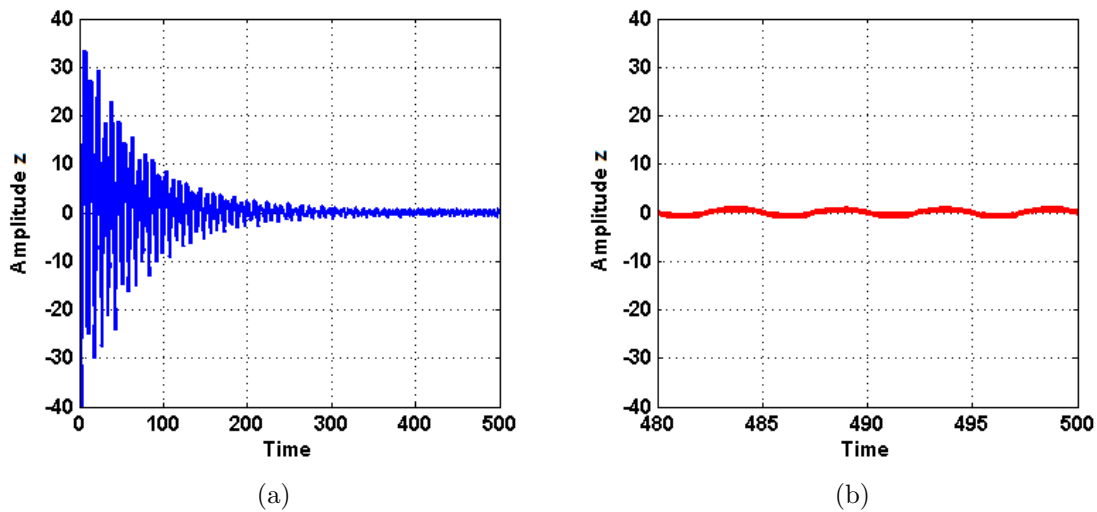


Figure 12: The OWTT vibrations after control at $\beta_1 = 5, \beta_2 = 0.5, \omega_1 = 1.26$ (a) all-round response, (b) last 20 seconds of the all-round response

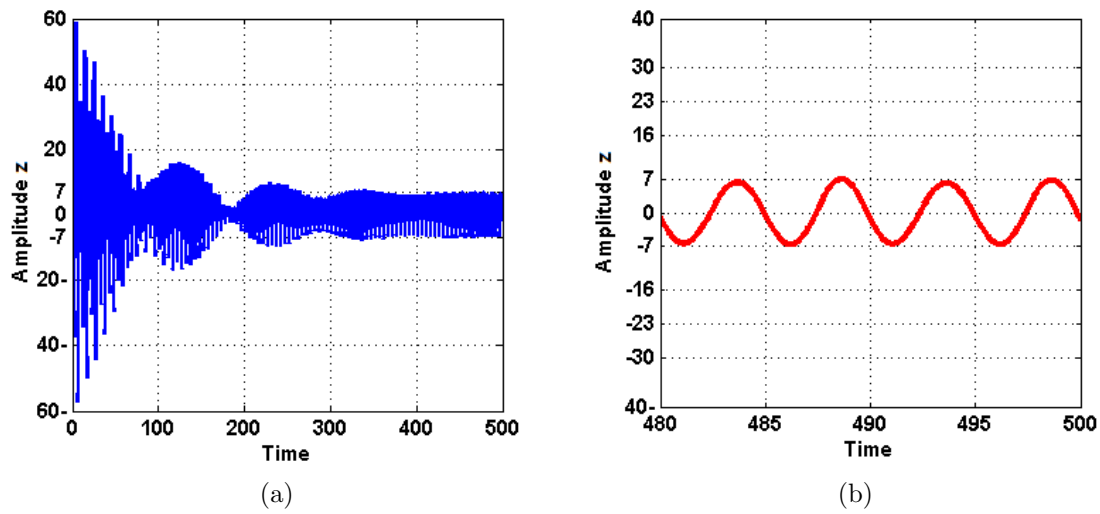


Figure 13: The OWTT vibrations after control at $\beta_1 = 5, \beta_2 = 0.05, \omega_1 = 1.26$ (a) all-round response, (b) last 20 seconds of the all-round response

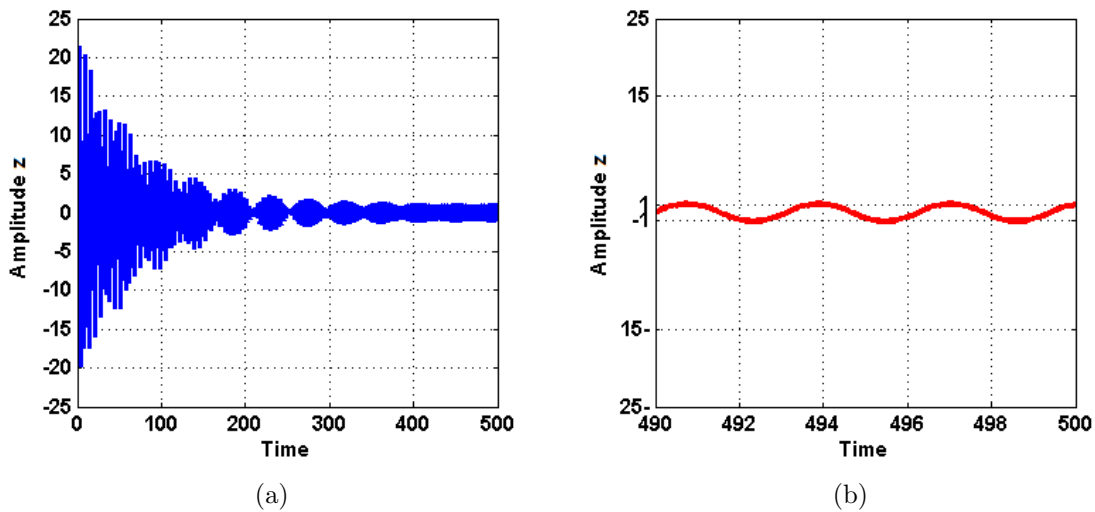


Figure 14: The OWTT vibrations after control at $\beta_1 = 5, \beta_2 = 0.5, \omega_1 = 2.01$ (a) all-round response, (b) last 20 seconds of the all-round response

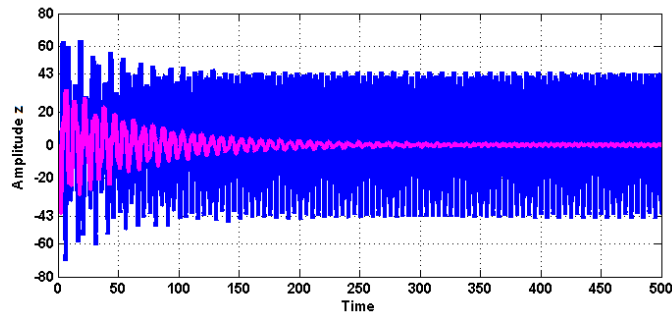
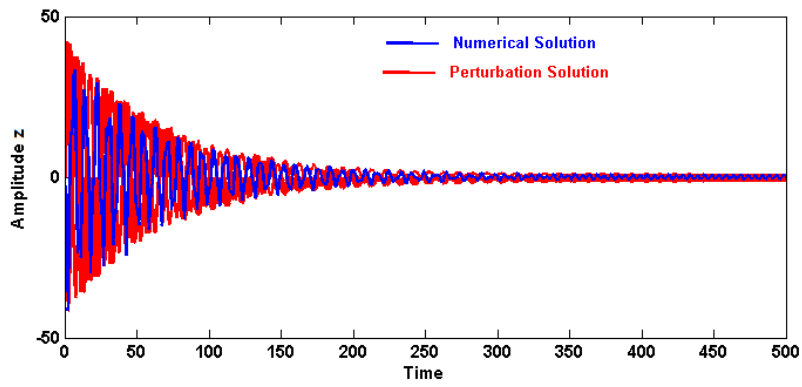


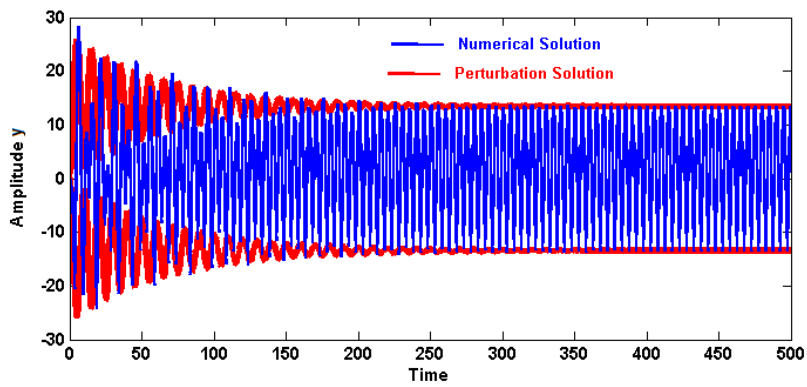
Figure 15: Energy flow between uncontrolled and controlled systems occurs at $\Omega_1 = \omega_1 = \omega_2 = 1.26$

6.1. Comparison of analytical and numerical simulation

As illustrated in Figures 16 and 17, this subsection compares numerical simulation for the controlled system of equation (2) with perturbation solutions of equations (17) and (18) at various values of the controller values β_1 and β_2 at primary and internal resonance $\Omega_1 = \omega_1 = \omega_2$. While the blue line denotes numerical integration, the red line represents the perturbation solution. These graphs show good agreement between the analytical and numerical simulation results. Figs. 17(a) and 18(a) represent the system response after control, but Figs. 17(b) and 18(b) represent the controller response.

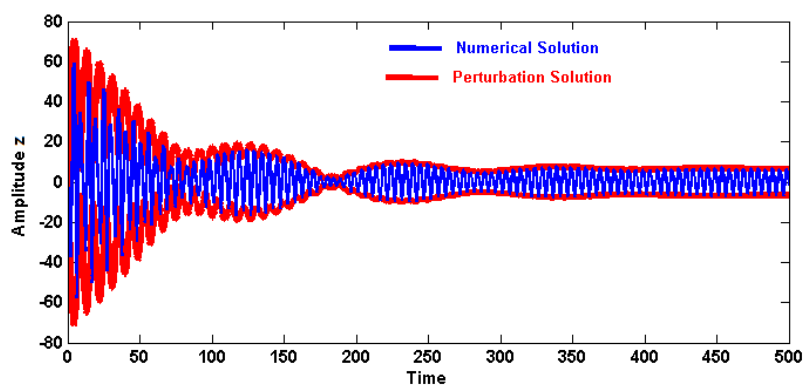


(a)

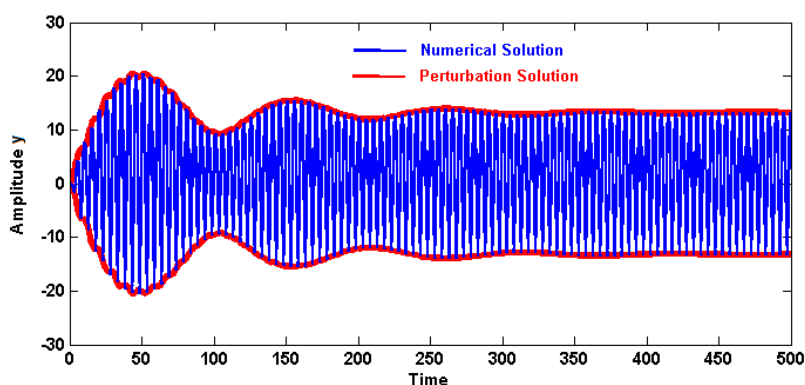


(b)

Figure 16: Comparison of the controlled system’s analytical and numerical simulations at $\beta_1 = 5, \beta_2 = 0.5, \omega_1 = 1.26$ (a) system response, (b) control response.



(a)



(b)

Figure 17: Comparison of the controlled system's analytical and numerical simulations at $\beta_1 = 5, \beta_2 = 0.05, \omega_1 = 1.26$ (a) system response, (b) control response.

6.2. The Poincaré maps

This section examines stability and uses Poincaré maps to plot bifurcation diagrams. These maps are used to transform the complex response in phase space to a discrete map in the lower dimensional space. Figures 18 and 19 analyzed the wind turbine behavior under the simultaneous primary and internal resonance case $\Omega_1 \approx \omega_1, \omega_1 \approx \omega_2$ using different values of control unit parameters β_1, β_2 with response and Poincaré map, respectively. Figure 18(a, b) demonstrates how the system begins with a chaotic reaction before stabilizing and exhibiting periodic motion on Poincaré's maps at $\beta_1 = 0, \beta_2 = 0$. The controlled system has a quasi-periodic motion at $\beta_1 = 5, \beta_2 = 0.5$, as depicted in Figure 19(a, b).

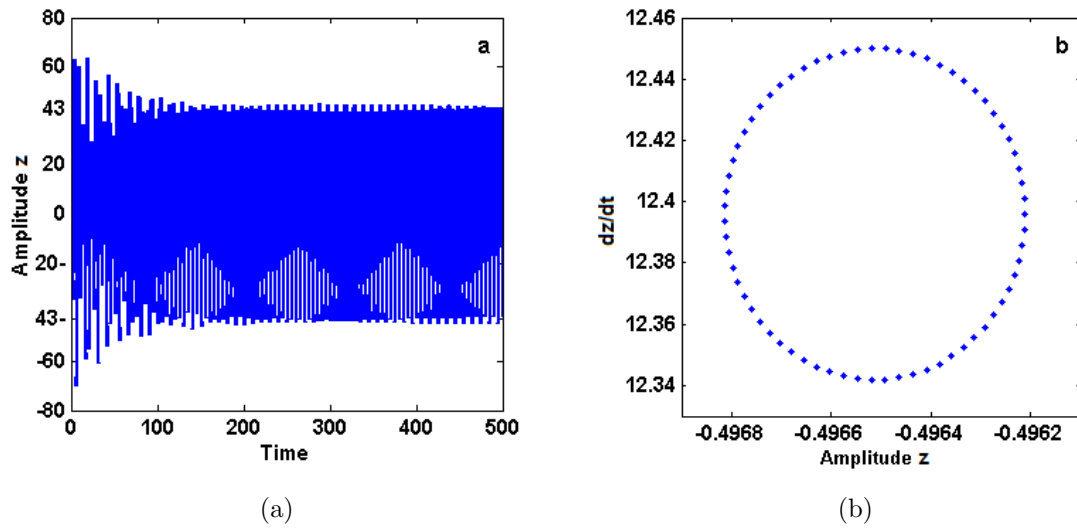


Figure 18: (a)Time responses of the system before control, (b) Poincaré ´ maps of the system before control at $\beta_1 = 0, \beta_2 = 0, \omega_1 = 1.26, \sigma_1 = 0, \sigma_2 = 0,$

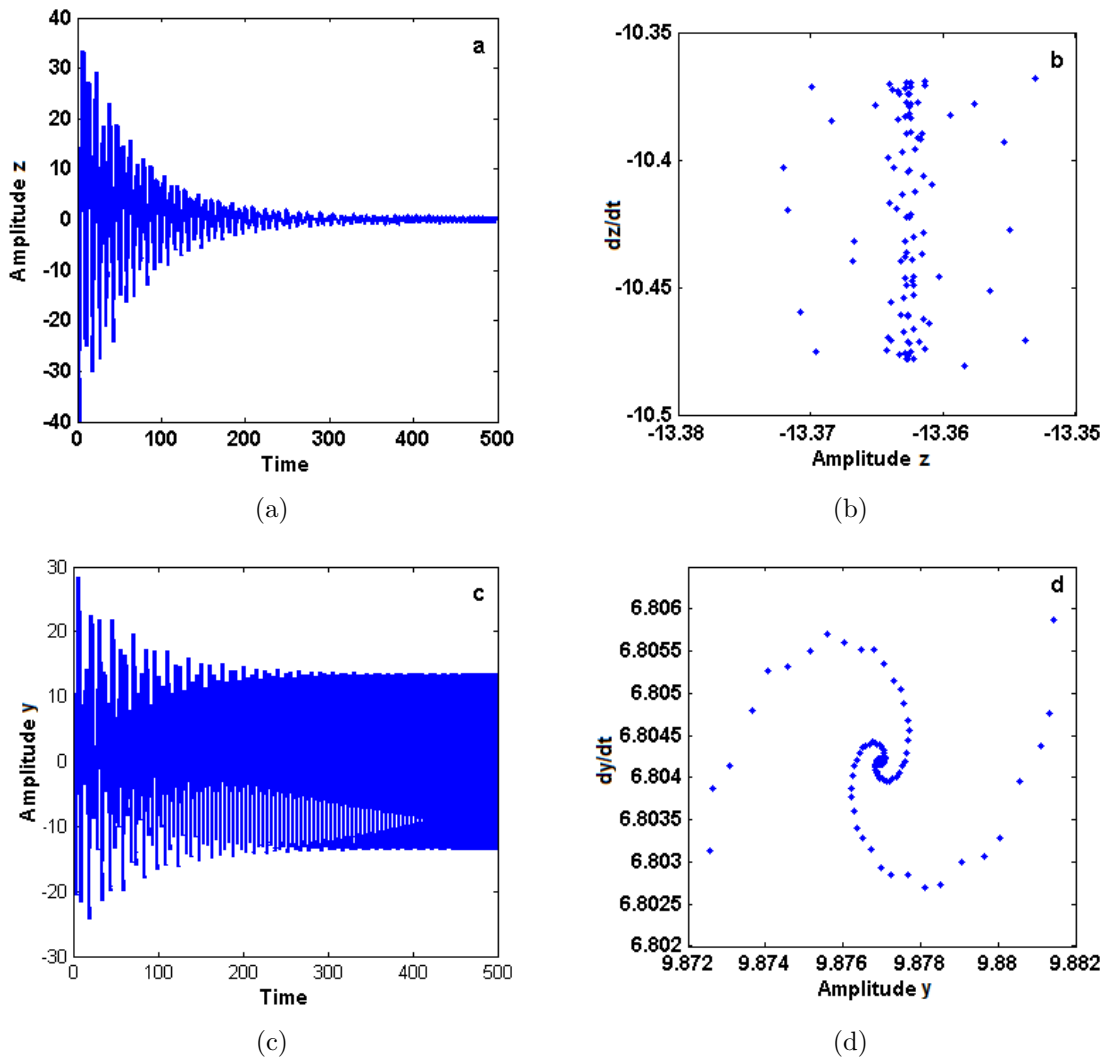


Figure 19: (a) Time responses of the system after control (b) Poincaré maps of the system after control (c) Time responses of the controller (d) Poincaré maps of the controller at $\beta_1 = 5, \beta_2 = 0.5, \omega_1 = 1.26, \sigma_1 = 0, \sigma_2 = 0$.

6.3. Comparison with published works

In comparison to previous studies, Dagli et al. [10] performed a dynamic vibration analysis for the single degree of freedom (SDOF) equation of motion using Rayleigh's energy. Hamed et al. [12] used an NPD controller to suppress the OWTT system's behavior with multiple external and parametric excitation forces. To analyze the response and stability, the averaging method is used. The steady oscillations of the wind turbine had been reduced from their former state by about 91 and the effectiveness of control is

$E_a=12$. With this work, the dynamics behavior and stability of the offshore wind turbine system with external excitation and applying PPF controller are studied. The steady oscillations of the wind turbine had been reduced from their former state by about 98.5 and the effectiveness of control is $E_a=72$.

7. Concluding Remarks

This study proposed a PPF controller to mitigate the offshore wind turbine tower model's nontrivial oscillations. Using the multiple time scale method, the equation of motion has been approximately solved. Using the phase plane technique, frequency response equations, and Poincare maps, the stability at worst resonance cases will be checked and analyzed. The whole work results can be summarized as follows:

- 1 . Before control, the wind turbine caused strong vibrations and jumps due to the existence of bifurcation points. after control, the wind turbine showed stable solutions without jumps due to the absence of bifurcation points.
- 2 . The wind turbine vibrations reached minimum levels in the range $\sigma_1 \in [-0.3, 0.3]$ especially at $\sigma_1=0$.
- 3 . Wind turbines operates safely in the range $\sigma_1 \in [-0.65, 0.65]$ when $\sigma_1 = \sigma_2$.
- 4 . Before control, the amplitude is 43 and after applying PPF control the amplitude become 0.6 then the effectiveness of control is $E_a=72$.
- 5 . The control signal gain β_1 and the feedback signal gain β_2 can be used to change the minimum amplitudes bandwidth.
- 6 . The wind turbine vibration amplitudes are very sensitive to the wind force amplitude of f_a before and after control and it is reasonable to channel most of the vibration energy to the controller.
- 7 . The steady oscillations of the wind turbine had been reduced from their former state by about 98.5.
- 8 . The controller damping μ_1 and μ_2 and natural frequencies ω_1 and ω_2 are inversely proportional with the minimum vibratory level reached at $\sigma_1 = \sigma_2$.
- 9 . Energy is moved from the system before control to the system after adding control at varying values ω_1, ω_2 and Ω_1 .
- 10 . Saturation phenomenon exhibit with change values of the control parameters β_1 and β_2 .
- 11 . On Poincare's maps, periodic motion may be seen before control and a quasi-periodic motion appear control.

Funding: This research did not receive any specific external funding other than the funding by the Deanship of Scientific Research, Taif University, Saudi Arabia with Project Number (1-443-1).

Acknowledgements

This research was supported by the Deanship of Scientific Research, Taif University, Saudi Arabia with Project Number (1-443-1).

Conflicts of Interest: The authors declare no conflict of interest.

References

- [0] M. A. Silva, J. S. Arora, and R. M. Brasil, “Formulations for the optimal design of RC wind turbine towers,” in Proceedings of the International Conference on Engineering Optimization (EngOpt 2008), Rio de Janeiro, Brazil, June 2008.
- [0] W. Shi, J. Han, C. Kim, D. Lee, H. Shin, and H. Park, “Feasibility study of offshore wind turbine substructures for southwest offshore wind farm project in Korea,” *Renewable Energy*, vol. 74, pp. 406–413, 2015.
- [0] C. Van der Woude and S. Narasimhan, “A study on vibration isolation for wind turbine structures,” *Engineering Structures*, vol. 60, pp. 223–234, 2014.
- [0] S. Bisoi and S. Haldar, Dynamic analysis of offshore wind turbine in clay considering soil–monopile–tower interaction, *Soil Dynamics and Earthquake Engineering* 63 (2014) 19–35.
- [0] F. Shi and R. Patton, “An active fault tolerant control approach to an offshore wind turbine model” *Renewable Energy* 75 (2015) 788-798
- [0] V. Nguyen Dinh and B. Basu, “Passive control of floating offshore wind turbine nacelle and spar vibrations by multiple tuned mass dampers” *Structural Control and Health Monitoring*. 22 (2015) 152-176.
- [0] Y. Hu and E. He, “Active structural control of a floating wind turbine with a stroke-limited hybrid mass damper” *Journal of Sound and Vibration* 410 (2017) 447-472.
- [0] S. A. Eisa, W. Stone and K. Wedeward, “Mathematical analysis of wind turbines dynamics under control limits: boundedness, existence, uniqueness, and multi time scale simulations” *International Journal of Dynamics and Control* 6 (2018) 929–949.
- [0] B. Fitzgerald , S. Sarkar and A. Staino, “Improved reliability of wind turbine towers with active tuned mass dampers (ATMDs)” *Journal of Sound and Vibration* 419 (2018) 103–122.

- [0] B. Y. Dagli , Y. Tuskan and U. Gokkus, "Evaluation of Offshore Wind Turbine Tower Dynamics with Numerical Analysis" *Advances in Civil Engineering* 2018 (2018) Article ID 3054851, 11 pages.
- [0] Y.S. Hamed, Ayman A. Aly, B. Saleh, Ageel F. Alogla, Awad M. Aljuaid, and Mosleh M. Alharthi "Vibration performance, stability and energy transfer of wind turbine tower via PD controller" *Computers, Materials & Continua*, 64(2) (2020) 871-886.
- [0] Y.S. Hamed, Ayman A. Aly, B. Saleh, Ageel F. Alogla, Awad M. Aljuaid, and Mosleh M. Alharthi "Nonlinear Structural Control Analysis of an Offshore Wind Turbine Tower System" *Processes* 8(1) (2020) 1-15.
- [0] Khadijah M. Abualnaja, Y. A. Amer, A. T. El-Sayed, E. El Emam Ahmed and Y. S. Hamed, Response Analysis and Controlling the Nonlinear Vibration of Van Der-Pol Duffing Oscillator Connected to the NIPPF Controller, *IEEE journal*, Vol. 9, 91836 - 91849, 17 June 2021
- [0] M. P. Cartmell, *Introduction to Linear, Parametric and Nonlinear Vibrations*. Chapman & Hall, London (1990).
- [0] A. H. Nayfeh and B. Balachandran, *Applied Nonlinear Dynamics: Analytical, Computational and Experimental Methods*. Wiley, New York (1995).
- [0] A. H. Nayfeh, *Problems in Perturbation*. Wiley, New York (1985).
- [0] Nayfeh, A., Mook, D.: *Nonlinear Oscillations*. Wiley, New York (1995).
- [0] Y. S. Hamed, K. M. Albogamy and M. Sayed, A proportional derivative (PD) controller for suppression the vibrations of a contact-mode AFM model, *IEEE ACCESS*, 8 (2020).
- [0] Y. S. Hamed and Ali Kandil, Influence of time delay on controlling the nonlinear oscillations of a rotating blade, *Symmetry* 2021, 13, 85.
- [0] Ali Kandi and Y. S. Hamed, Tuned Positive Position Feedback Control of an Active Magnetic Bearings System With 16-Poles and Constant Stiffness, *IEEE ACCESS*, 9 (2021).
- [0] Kandil, A., Hamed, Y.S., Alsharif, A.M., Awrejcewicz, J.: 2D and 3D Visualizations of the Mass-Damper-Spring Model Dynamics Controlled by a Servo-Controlled Linear Actuator. *IEEE Access*. 9, 153012–153026 (2021).
- [0] Kandil, A., Hamed, Y.S., Awrejcewicz, J.: Harmonic Balance Method to Analyze the Steady-State Response of a Controlled Mass-Damper-Spring Model. *Symmetry* 2022, 14, 1247.

- [0] Kandil, A., Hamed, Y.S., Abualnaja, Khadijah M., Bednarek, Maksymilian., Awrejcewicz, J.:1/3 Order Subharmonic Resonance Control of a Mass-Damper-Spring Model via Cubic-Position Negative-Velocity Feedback. *Symmetry* 2022, 14,685.
- [0] Carl M. Bender, Steven A. Orszag, *Advanced Mathematical Methods for Scientists and Engineers I*. Springer New York, NY (1999).
- [0] S. Boi, A. Mazzino, and J. O. Pralits, Minimal model for zero-inertia instabilities in shear-dominated non-Newtonian flows, *Physical Review E* 88, 033007 (2013).
- [0] Arash Hemmati, Erkan Oterkus and Mahdi Khorasanchib, Vibration suppression of offshore wind turbine foundations using tuned liquid column dampers and tuned mass dampers *Ocean Engineering*, 172 (2019) 286–295.
- [0] J. Yang, E.M. He and Y.Q. Hu, Dynamic modeling and vibration suppression for an offshore wind turbine with a tuned mass damper in floating platform, *Applied Ocean Research* 83 (2019) 21–29.
- [0] Tian Li, Zhenqing Liu, Shujie Liu, Yicheng Fan, Qingshan Yang and Hongdi Xiao, Numerical study on passive structural control of semi-submersible floating wind turbine considering non-collinear wind and waves, *Ocean Engineering* 266 (2022) 112745.
- [0] Valentina Laface, Gioacchino Alotta, Giuseppe Failla, Carlo Ruzzo and Felice Arena, A two-degree-of-freedom tuned mass damper for offshore wind turbines on floating spar supports, *Marine Structures* 83 (2022) 103146.
- [0] Zili Zhang, Vibration suppression of floating offshore wind turbines using electromagnetic shunt tuned mass damper, *Renewable Energy* 198 (2022) 1279–1295.

Appendix

The elements r_{ij} ($i, j = 1, \dots, 4$) of the Jacobian matrix J given in Eq. 26

$$r_{11} = -\frac{\mu_1}{2}, r_{12} = \frac{f_a}{2\omega_1} \sin\theta_{10}, r_{13} = \frac{\beta_1}{2\omega_1} \sin\theta_{20} \quad r_{14} = \frac{\beta_1 a_{20}}{2\omega_1} \cos\theta_{20}$$

$$r_{21} = -\frac{\beta_1 a_{20}}{2\omega_1 a_{10}^2} \cos\theta_{20} + \frac{f_a}{2\omega_1 a_{10}^2} \sin\theta_{10}, r_{22} = -\frac{f_a}{2\omega_1 a_{10}} \cos\theta_{10}, r_{23} = \frac{\beta_1}{2\omega_1 a_{10}} \cos\theta_{20},$$

$$r_{24} = -\frac{\beta_1 a_{20}}{2\omega_1 a_{10}} \sin\theta_{20}$$

$$r_{31} = -\frac{\beta_2}{2\omega_2} \sin\theta_{20}, r_{32} = 0, r_{33} = -\frac{\mu_2}{2}$$

$$r_{34} = -\frac{\beta_2 a_{10}}{2\omega_2} \cos\theta_{20}$$

$$r_{41} = -\frac{\beta_2}{2\omega_2 a_{20}} \cos\theta_{20} - \frac{\beta_1 a_{20}}{2\omega_1 a_{10}^2} \cos\theta_{20} + \frac{f_a}{2\omega_1 a_{10}^2} \sin\theta_{10}, \quad r_{42} = -\frac{f_a}{2\omega_1 a_{10}} \cos\theta_{10}$$

$$r_{43} = \frac{\beta_2 a_{10}}{2\omega_2 a_{20}^2} \cos\theta_{20} + \frac{\theta_1}{2\theta_1 a_{10}} \cos\theta_{20},$$

$$r_{44} = \frac{\beta_2 a_{10}}{2\omega_2 a_{20}} \sin\theta_{20} - \frac{\beta_1 a_{20}}{2\omega_1 a_{10}} \sin\theta_{20}$$

The elements R_i ($i = 1, \dots, 4$) of Eq. 27: $R_1 = -\sum_{i=1}^4 r_{ii}$

$$R_2 = \frac{1}{2!} \sum_{i=1}^4 \sum_{j=1}^4 r_{ii} r_{jj} - r_{ij} r_{ji}$$

$$R_3 = -\frac{1}{3!} \sum_{i=1}^4 \sum_{j=1}^4 \sum_{k=1}^4 r_{ii} r_{jj} r_{kk} - 3r_{ii} r_{jk} r_{kj} + 2r_{ij} r_{jk} r_{ki}$$

$$R_4 = \frac{1}{4!} \sum_{i=1}^4 \sum_{j=1}^4 \sum_{k=1}^4 \sum_{l=1}^4 r_{ii} r_{jj} r_{kk} r_{ll} - 6r_{ii} r_{jj} r_{kl} r_{lk} + 8r_{ii} r_{jk} r_{kl} r_{lj} + 3r_{ij} r_{ji} r_{kl} r_{lk} - 6r_{ij} r_{jk} r_{kl} r_{li}$$